A Novel Topology Optimization of the Frame Mold for Composite Autoclave Process

Bo Yue[1] · Yingjie Xu[1,2] · Weihong Zhang[1]

Abstract

Frame mold is the key tool for autoclave processing of composite structures. Its stiffness and temperature uniformity have important influences on the quality, particularly the synchronization of curing of the processed composite structures. In this paper, a novel topology optimization method is proposed to design the frame mold for improving the stiffness and the temperature uniformity while reducing the weight. A computational fluid dynamics (CFD) model is developed to analyze the temperature field of the frame mold during the curing process and its accuracy is validated by experiment. Furthermore, the original mold and optimized mold covered with the composite panel are introduced to the numerical model to research the evolution process of the degree of cure (DoC) during a curing cycle. The results show that the overall structure weight of the optimized mold is reduced by 16.04%, the stiffness is increased by 27%, and the temperature uniformity is increased by 29%. The synchronization of curing of the composite panel is also improved by 26.7% using the optimized mold.

Nomenclature

x	Pseudo-density variable vector
Ω	Design domain of the mold
f	External load
u	Nodal displacement
$|\Omega|$	Volume of the design domain
E_i	Elastic modules of element i
E_0	Elastic modules of the solid material
p	Penalization factor
k_0	Stiffness matrix of the solid material

✉ Yingjie Xu
  xu.yingjie@nwpu.edu.cn

1 State IJR Center of Aerospace Design and Additive Manufacturing, Northwestern Polytechnical University, Xi'an, Shaanxi 710072, China

2 Shaanxi Engineering Laboratory of Aerospace Structure Design and Application, Northwestern Polytechnical University, P.O. Box 68, Xi'an, Shaanxi 710072, China

$r_{\min}$	Filter radius
ρ	Density
p	Pressure of fluid
$\mathbf{S}$	Generalized source terms of the momentum equation
$h(p, T)$	Function of fluid pressure and temperature
S_h	Internal heat source
D	Hydraulic diameter
α	Degree of cure
K_i	Curing rate constant
A_i	Frequency factor
$\dot{q}$	Heat released in the cure reaction
H_r	Heat generated by the complete reaction of unit mass of resin
n_D	The number of the design variables
$f(\mathbf{x})$	Global elastic strain energy
$\mathbf{G}$	Self-weight load
$\mathbf{K}$	Structural global stiffness matrix
β	Volume fraction
m_i	Mass of element i
m_0	Mass of the solid material
k_i	Stiffness matrix of the element i
N_e	Neighborhood elements set of the element e
H_{ei}	Convolution operator
μ	Dynamic viscosity
$\mathbf{v}$	Velocity vector
λ	Thermal conductivity
Φ	Energy of viscous dissipation
U	Average velocity of fluid
Re	Reynolds number
$\frac{d\alpha}{dt}$	Instantaneous cure rate
R	Universal gas constant
ΔE_i	Activation energy
V_r	Volume fraction of the resin

Acronyms and Abbreviations

CFD	Computational fluid dynamics
HTC	Heat transfer coefficient
UDF	User defined function
DoC	Degree of cure
SIMP	Solid Isotropic Material Penalization

1 Introduction

Fiber reinforced thermoset matrix composites have been widely used in aerospace applications due to their high specific stiffness and strength. Autoclave curing process is a commonly used method for manufacturing thermoset matrix composite parts, especially the primary load-bearing parts in aerospace industries [1]. The mold is the pivotal tool to ensure the composite parts can be cured according to their designed geometries [2]. The

frame mold is mainly used for the curing of large thin-walled composite parts, such as skins, stiffened panels of wing and fuselage. A typical frame mold usually consists of two main components [3], a mold plate shaped to the product contour and a substructure, as shown in Fig. 1. The performance of a frame mold should generally satisfy the following requirements: (a) Excellent temperature uniformity to improve the synchronism of curing in autoclave process [4]. The excessive temperature difference will lead to a large deviation of DoC and thermal residual stresses in composite, which has an adverse effect on the mechanical properties of the cured parts [5–10]. (b) High stiffness to reduce the deformation of mold during the curing and transportation. (c) Lightweight to reduce the installation and transportation cost [4].

A reasonable design of frame mold is important for improving the quality of composite parts. In the design, numerical simulation is an efficient tool to evaluate the performance of the mold. The simulation model based on CFD is widely used for predicting the temperature distribution of the mold during the autoclave process [11–13]. Xie et al. [14, 15] took the consideration of auxiliaries and composite parts into the CFD simulation and found the curing exothermic reaction of composite has a slight influence on the temperature distribution of the mold. Zhang et al. [16] investigated the influences of the material of mold and fluid on the temperature uniformity of the mold. The results showed that a mold material with high thermal conductivity and a fluid with high specific heat capacity and thermal conductivity will improve the heating rate and temperature uniformity of the mold. Besides, Weber et al. [17] developed a semi-empirical approach using shift factors in combination with a measured reference curve to estimate the temperature distribution of the mold in autoclave process. In this way, the computation cost is significantly reduced compared to the CFD simulations. Hudek [3] adopted this method to study the influences of the vacuum bag, the position of the mold, and the heat flow direction on the heat transfer in autoclave. The results indicated that the heat transfer coefficient (HTC) in the front and the back of an autoclave has a significant difference.

Comparing with the number of studies on the thermal analysis of the autoclave mold, there are few studies on the optimization of mold. Due to the complexity and the poor aerodynamics of the shape of frame mold substructure, shadowing effect [3, 18] occurs during
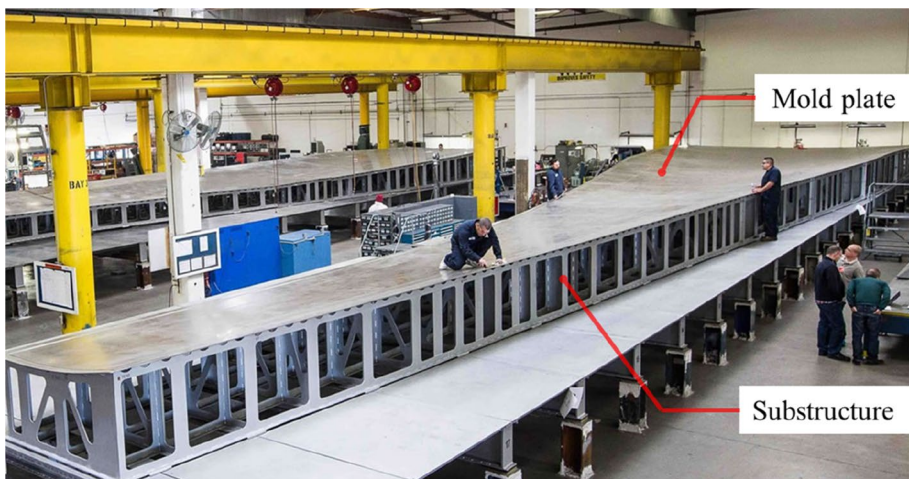

Fig. 1 The frame mold for a composite wing (https://ascentaerospace.com)

autoclave process and leads to a delay of heating rate and the temperature gradient. Especially for the large molds with excessive substructures, the flow velocity is significantly reduced when fluid passes through the mold. Studies [19] have shown that the thermal performance of the mold is strongly affected by the geometric features of substructure, such as the shape and area of the ventilation holes, the arrangement and thickness of grid-boards. It is noted that these geometric parameters usually have an opposite influence on the temperature uniformity and stiffness of mold. For example, the increase of the area of ventilation holes will effectively improve the mold temperature uniformity and reduce the mold weight. However, the stiffness of the mold is obviously reduced.

Therefore, it is costly and time-consuming to get a mold structure with great thermal performance under the constraints of stiffness by traditional trial and error. An optimization method that combines the numerical simulation with a genetic algorithm was proposed by Wang et al. [20] to find the optimal parameters of the mold substructure. Another mold for a composite C spar was optimized [21] by the same approach and the maximum difference in DoC is decreased by 40.16%. However, there are several disadvantages linked to such a genetic algorithm optimization method. Firstly, the initial range and increment of the design parameters are difficult to define, which has a significant influence on the optimization result. Secondly, a large number of simulations are involved during the design iteration. An iterative analysis has to be carried out for each new situation. This is extremely time-consuming and computationally expensive. Besides, the traditional structural configuration of the mold continues to use in optimization, and it is unable to get an innovative structure with better performance.

Thus, it is important to find a more efficient way to resolve the contradiction between the temperature uniformity and stiffness of mold. This paper is aimed at presenting a novel topology optimization design method of the substructure of frame mold to achieve better temperature uniformity and stiffness. The topology optimization formulation is firstly developed for the frame mold in autoclave process and a novel configuration of the substructure is obtained. The optimal mold is manufactured and tested in an autoclave. The numerical simulations of the elastic and thermal performances of the original and optimized mold are conducted respectively. Furthermore, auxiliary materials and composite part are considered in the simulation to verify the performance of the optimized mold.

2 Topology Optimization Model of Frame Mold

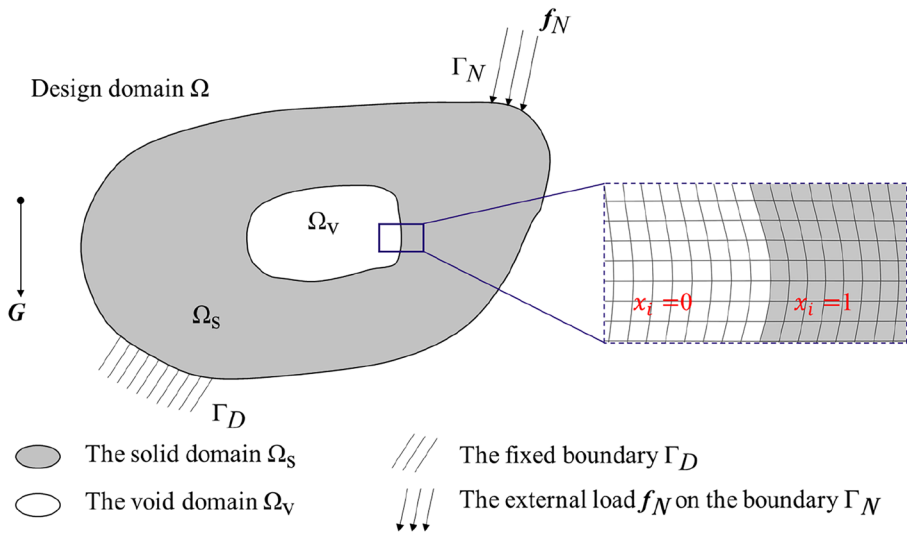### 2.1 Formulation of the Topology Optimization

Topology optimization [22] is a method that designs the material distribution in an optimal way to get an innovative structure. It originates from the field of solid mechanics and has been widely applied and developed over the past three decades [23, 24]. Topology optimization has been recognized as an effective tool for lightweight and performance design in engineering structures [25]. In practical structural design processes, the deformation control problem of a loaded structure is usually presented with limited material consumption. These problems are primarily formulated as the standard compliance-based topology optimization, with the objective function of minimizing the compliance of the structure, the constraints of the volume fraction of design domain, loads and boundary conditions. In this way, a structure with stiff conceptual material layout will be provided by the optimized result and it provides guidance for the optimization of the structure.

　　Based on the characteristics of topology optimization and the design requirement of frame mold, the mold optimization problem can be considered as standard compliance-based topology optimization. The temperature uniformity of the frame mold is strongly related to the volume fraction of ventilation holes. Therefore, the design goals of the high stiffness and temperature uniformity of frame mold can be achieved by setting the objective function of minimizing global compliance and the constraint of the volume fraction of ventilation holes.

　　In the present study, the density-based topology optimization method is adopted and the schematic diagram of the analysis domain including the definitions of boundaries is displayed in Fig. 2. The concept of pseudo-density field (x) in the [0,1] domain is proposed by Bendsoe [22] and used to describe the distribution of material in the design domain. $x =$ 0 corresponding to a void, $x = 1$ to solid and $0 < x < 1$ to the porous material with voids at a micro level. For generally mechanical structural problems under statics, the density-based compliance topology optimization can be formulated as follows:

$$\begin{aligned}
&\text{Find:} && \boldsymbol{x} = (x_1, x_1, ..., x_i, ..., x_{n_D}), && i = 1, 2, ..., n_D \\
&\text{Minimize:} && f(\boldsymbol{x}) = \tfrac{1}{2}\boldsymbol{F}^T\boldsymbol{u} \\
&\text{Subject to:} && \int_\Omega x_i d\Omega / |\Omega| \le \beta && \text{Volume fraction constraint} \\
& && 0.01 \le x_i \le 1 && \text{Design variable bounds} \\
& && \left.\begin{array}{ll} \boldsymbol{F} = \boldsymbol{f} + \boldsymbol{G} = \boldsymbol{Ku} & \text{in } \Omega \\ \boldsymbol{u} = \boldsymbol{u}_D & \text{on } \Gamma_D \\ \boldsymbol{f} = \boldsymbol{f}_N & \text{on } \Gamma_N \end{array}\right\} & \text{Governing equations}
\end{aligned} \tag{1}$$

where $\boldsymbol{x}$ is the pseudo-density variable vector containing n_D element-based design variables x_i, describing the material layout in the design domain Ω. When x_i is close to 1 or 0 represents a solid or a void finite element respectively. Meanwhile, the lower bound of

Fig. 2 Schematic diagram of the analysis domain including the definitions of boundaries in topology optimization

the pseudo-density variables is limited to 0.01 to prevent the singular stiffness matrix. The maximum structural stiffness, i.e., minimum structural compliance, it is usually evaluated with the objective function of minimizing the global elastic strain energy $f(x)$. The strain energy is expressed by the external load f, the self-weight load G, and the nodal displacement u. K is the structural global stiffness matrix. Normally, $|\Omega|$ denotes the volume of the design domain and the upper bound of the volume fraction β is prescribed to limit the volume occupied by the solid. In the optimization of the frame mold, the volume fraction of ventilation holes can be defined by $1-\beta$.

In addition to indicating the absence or presence of material, the pseudo-density is corresponding to the physical properties of the material in an interpolation model. At the same time, the interpolation model needs to be penalized in a proper way to guarantee a clear design result. Because of the simplicity of the Solid Isotropic Material Penalization (SIMP) interpolation scheme [26] in both conception and numerical implementation, this method has been applied generally in topology optimization. Material properties, such as the elasticity modulus, is interpolated with respect to the pseudo-density field in the following expression:

$$E_i = x_i^p E_0$$
$$m_i = x_i m_0 \tag{2}$$

where E_i and m_i are the element elastic modules and mass, respectively. E_0 and m_0 are the corresponding element elastic modules and mass when the element is a solid one. p is the penalization factor for adjusting the shape of E_i and is usually assigned as a value larger than 1, as shown in Fig. 3.

The stiffness matrix of the element has a linear correlation with its elastic modulus, so there is a function similar to Eq. (2):

$$k_i = x_i^p k_0 \tag{3}$$

where k_i and k_0 is the stiffness matrix of the element i and the solid material with the pseudo density of 1 respectively. p is assigned as 3 in this paper. The stiffness of the elements with the intermediate density value will be penalized to a rather small value by this power law

Fig. 3 Interpolation function for different values of the penalization factor p
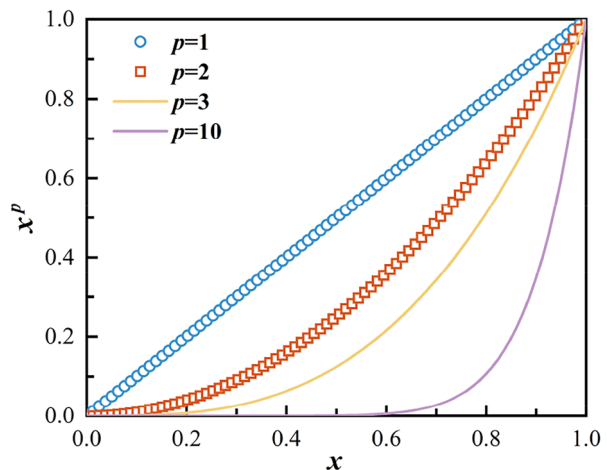
scheme and the fuzzy porous elements will be eliminated. By redistributing, the pseudo-density of optimization result will be driven towards 0 or 1 during optimization.

However, the checkerboard patterns, mesh-dependency, and local minima are usually encountered in the density-based approaches [27]. To prevent these numerical instabilities, the sensitivity filtering scheme and density filtering scheme are proposed by researchers [28, 29]. Both of the two filter models are based on the weighted average of the sensitivity or density of all elements within the filter radius. Hence, the filtered sensitivity and density are calculated as:

$$\frac{\partial f}{\partial x_e} = (x_e)^{-1} \frac{1}{\sum\limits_{i=1}^{N_e} H_{ei}} \sum_{i=1}^{N_e} H_{ei} x_i \frac{\partial f}{\partial x_i} \tag{4}$$

$$x_e = \frac{1}{\sum\limits_{i=1}^{N_e} H_{ei}} \sum_{i=1}^{N_e} H_{ei} x_i \tag{5}$$

$$H_{ei} = r_{\min} - dist(e, i), N_e = \left\{ i \middle| dist(e, i) \leq r_{\min} \right\} \tag{6}$$

where N_e denotes the neighborhood elements set of the element e within a certain filter radius $r_{\min}$ and the convolution operator (weight factor) H_{ei} is defined based on the distance between the element e and i. It is seen that with the distance $dist(e, i)$ reducing, the convolution operator for element i decays linearly.

2.2 Topology Optimization Model

The frame mold for autoclave process of a composite panel is concerned in the topology optimization. The geometry of the original mold is shown in Fig. 4. The size of mold is 3 m in length, 1.2 m in width, and 0.4 m in height. The mold plate has a curvature surface. The radius of curvature is 4 m, and the thickness is 9 mm for the mold plate. The substructure of
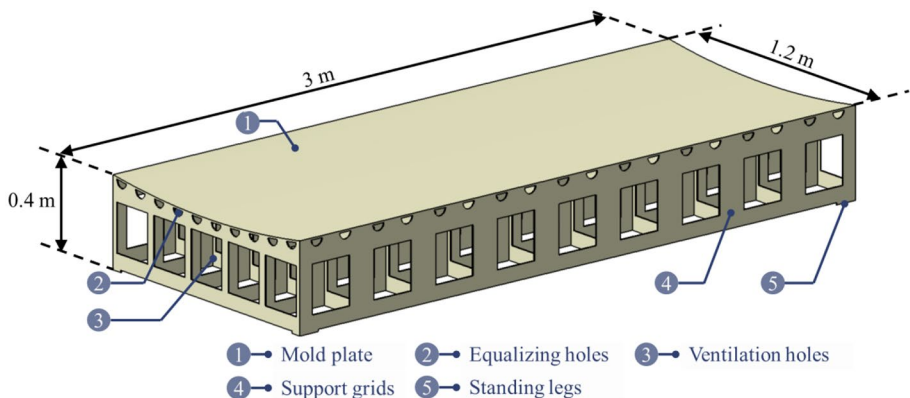

Fig. 4 Geometry of the original mold

the mold contains four parts: ventilation holes, support grids, equalizing holes and standing legs. The number of support grids in width and length are 6 and 10, respectively. The thickness of support grids is 5 mm. The dimension of ventilation holes is 200 mm × 220 mm and the radius of equalizing holes is 30 mm.

The material of the mold is invar alloy, which is widely used for the mold of aircraft and aerospace composite parts due to its low coefficient of thermal expansion [30, 31]. The material properties of the invar alloy are listed in Table 1.

The definition of the design domain has an important influence on the topology optimization results. As shown in Fig. 5, the mold plate is defined as the non-design domain for maintaining the shape of the composite panel. The arrangement and the thickness of the support grids keep constant with the original mold. During the autoclave process, hot air mainly flows into the mold from the ventilation holes and transfers heat to the lower face of the mold plate. The relatively small channels called equalizing holes just help to improve the heat convection to avoid excessive thermal gradient locally, they are considered to be invariable in traditional optimization design [20]. However, the presence of equalizing holes significantly reduces the designability of the substructure. Therefore, the ventilation holes and equalizing holes are all filled with solids, and the 6 × 10 solid support grids are defined as the design domain.

During autoclave process, the deformation of mold contains two parts: (a) the elastic deformation caused by the self-weight and the uniform distributed compressive force from the composite panel and auxiliary materials (the autoclave pressure applied in the mold is balanced); (b) the thermal deformation generated by the temperature difference in heating and cooling stages. Therefore, the self-weight load, the compressive force from the composite panel and auxiliary materials, and the temperature difference (from room temperature to the dwelling temperature) are applied on the finite element model of the frame mold. One of the standing legs is totally fixed, and the others are fixed only in Z direction.

The topology optimization problem formulated in Eq. (1) is conducted in commercial software OPTISTRUCT based on the SIMP interpolation scheme. It is known that the increase of the volume fraction of ventilation holes would effectively improve the mold temperature uniformity. Thus, to achieve excellent temperature uniformity, a higher volume fraction of ventilation holes is demanded. The volume fraction of ventilation holes of the original mold is 44.3%. Thus, in this paper we have chosen a 70% volume fraction of ventilation holes, which is far higher than the original one to achieve an excellent temperature uniformity of the frame mold. Furthermore, the penalization factor p is assigned as 3 to prevent instabilities associated with the original grey starting guess. And to avoid extremely thin structural members and the checkerboard patterns, the radius r_{min} in the density filter is set to 3 times the average element size.

Table 1 Material properties of invar alloy

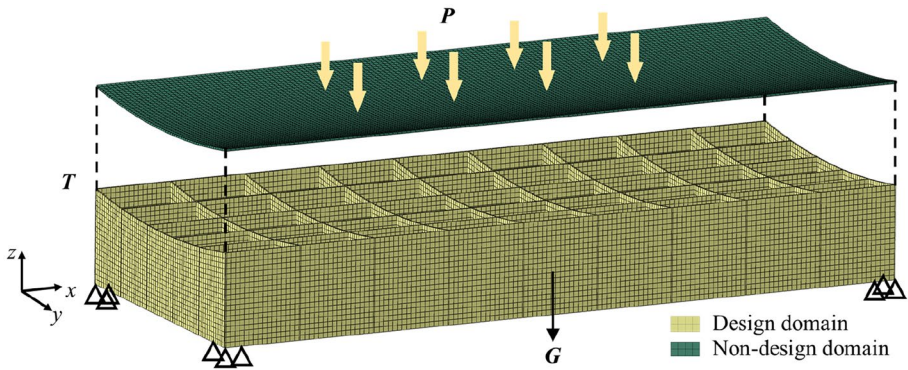| Parameters	value
Density/(kg·m^{-3})	8100
Elastic modulus/GPa	210
Poisson's ratio	0.25
Heat capacity/(J·kg^{-1}·K^{-1})	515
Conductivity/(W·m^{-1}·K^{-1})	11
Coefficient of thermal expansion/K^{-1}	1.8×10^{-6}

Fig. 5 Schematic of the topology optimization finite element model

2.3 Optimization Result

The optimized mold substructure with a clear topology configuration is shown in Fig. 6a, which eliminates the elements with the pseudo-density lower than 0.7. It is observed that the optimized result displays a symmetrical structure and breaks the limitation of the traditional structural configuration. The structural complexity is much higher than the original mold, including several arch-shaped configurations with excellent stiffness performance. Large ventilation holes are distributed on the support grids for facilitating the flow of air and increasing the heat convection between the mold and air. Considering the feasibility of the actual manufacturing of the frame mold, a reconstruction of the topology optimization result is conducted and illustrated in Fig. 6b.

The support grids of the reconstructed mold are manufactured by wire-electrode cutting, which are then welded with the mold plate. The manufactured mold scaled with the ratio of 3:1 is displayed in Fig. 7.

The weights of the optimized and original molds are computed and compared in Fig. 8. Compared with the original mold, the total weight and substructure weight of the optimized mold have been reduced by 16.04% and 33.6%, respectively. To evaluate the stiffness of the optimized mold, the deformations of mold in autoclave process are computed by finite element simulations. As shown in Fig. 8, the maximum deformation of the original
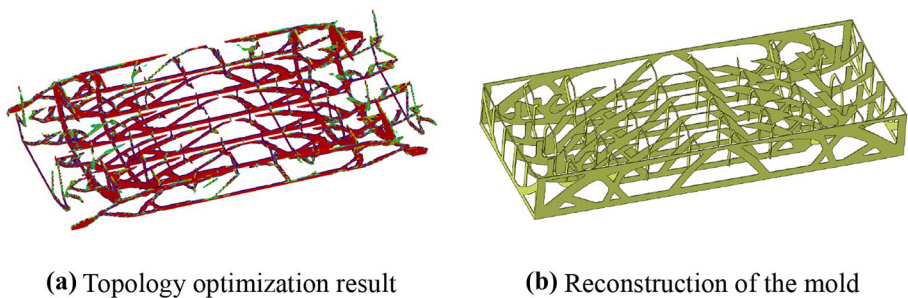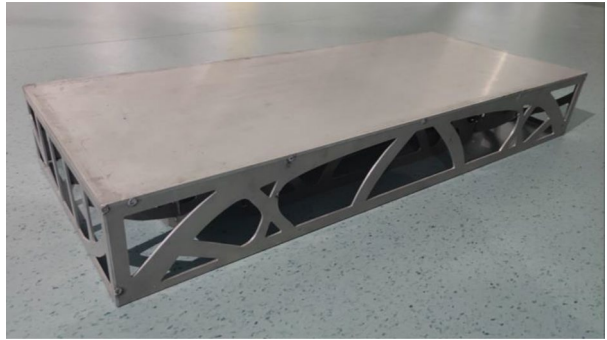

(a) Topology optimization result

(b) Reconstruction of the mold

Fig. 6 Topology optimized frame mold

Fig. 7 The manufactured mold

mold is 0.1415 mm while the optimal design is 0.1033 mm. The optimized mold shows a 27% increase in stiffness.

To evaluate the temperature uniformity of the optimized mold, a CFD simulation of autoclave process is conducted, and the manufactured mold is also tested in an autoclave. Details are presented in the following section.

3 Simulation and Experimental Test of Mold Temperature in Autoclave Process

3.1 Description of the Autoclave System

As shown in Fig. 9, the autoclave is a closed system with inner and outer cavities. During autoclave process, the fan located at the end of the outer cavity drives the air or noble gases to the lid along the duct where the electric resistance wires heating the air with a pre-scribed velocity controlled by the program. Then, the hot air blows from the door to the tail of the inner cavity to achieve a circulating flow. Meanwhile, heat is transferred to the mold and other parts by the media of the heated recirculating wind.

The heat transfer in the autoclave involves three parts: forced convection, heat conduction and thermal radiation. Since thermal radiation effect is considered unremarkable below 200 °C [32–34], the temperature distribution of thermoset composite (the curing temperature is usually lower than 200 °C) in autoclave process is mainly determined by the heat convection in fluid domains and heat conduction in solid domains.
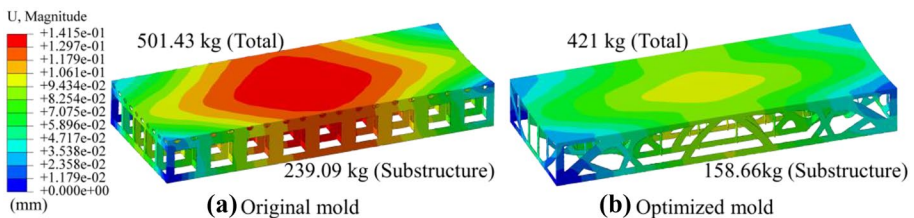
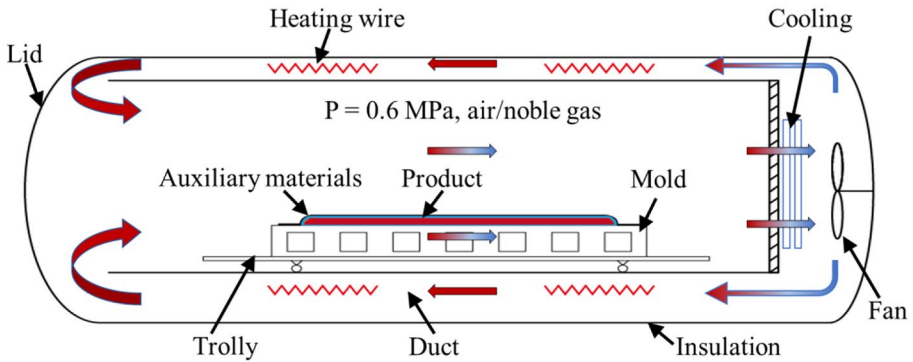**Fig. 8** Comparison of the weights and stiffness of the two molds

Fig. 9 The working principle of autoclave system

3.2 Governing Equations

3.2.1 Equations of the Heat Convection in Fluid Domains

The fluid flow and heat transfer in the autoclave should satisfy the following basic physics laws [14, 20]:

Mass conservation equation:

$$\frac{\partial \rho}{\partial t} + div(\rho v) = 0 \tag{7}$$

Momentum conservation equation:

$$\frac{\partial(\rho v)}{\partial t} + div(\rho v \otimes v) = div(\mu\, grad(v)) - grad(p) + S \tag{8}$$

where ρ, and μ and p are the density, dynamic viscosity and pressure of fluid respectively, $v = [u\ v\ w]$ denotes the velocity vector, S is the generalized source terms of the momentum equation.

Energy conservation equation:

$$\frac{\partial(\rho h)}{\partial t} + div(\rho h v) = div(\lambda\, grad(T)) - p\, div(v) + \Phi + S_{\mathrm{h}} \tag{9}$$

where $h = h(p, T)$ is expressed as a function of fluid pressure and temperature, λ is the thermal conductivity of fluid, Φ and S_{h} represent the energy of viscous dissipation and the internal heat source.

Since there are six unknown variables in Eqs. (7)–(9), a state equation correlating density ρ and pressure p is needed to close the equations:

$$\rho = f(p, T) \tag{10}$$

In autoclave process, since the heating of mold is realized through forced convection of fluid, the state of flow should be considered in simulation. To determine the type of flow,

the Reynolds number Re has to be defined. Re is a dimensionless parameter indicating the ratio between the inertial and the viscous forces in the flow.

$$Re = \frac{DU\rho}{\mu} \tag{11}$$

where U is the average velocity of fluid and D is the hydraulic diameter. The flow in the autoclave is considered laminar while $Re < 2300$ and turbulent while $Re > 12000$. Re between 2300 and 12000 represents a transition state from laminar to turbulent flow.

3.2.2 Equations of the Heat Conduction in Solid Domains

In the solid domain, the governing equation is relatively simple since heat conduction is the only pattern of heat transfer inside solid domain. The energy equation can be defined as

$$\frac{\partial(\rho_s c_s T)}{\partial t} = div\left(\lambda_s grad(T)\right) + S_T \tag{12}$$

where ρ_s, and c_s and λ_s are the density, specific heat, and thermal conductivity of solid respectively, S_T denotes the internal heat source of solid. In this study, S_T is none in the mold domain since there is not heat source inside the mold. However, S_T should be considered for the composite due to the exothermic reaction of resin curing. The reaction heat can be evaluated by the cure kinetic equation. Note that in order to have an intuitive observation of the mold temperature, in this section we consider a specific case in which only the mold is inside the autoclave. Composite panel and auxiliary materials are considered in the simulation in Sect. 4 for verifying the synchronism of curing. Details will be discussed in Sect. 4.

In this study, the commercial software ANSYS CFX is used to solve the above governing equations of fluid flow and heat transfer. The simulation process is transient, and the time step size is set as 60 s. The iterative is considered to be converged at every time step when the maximum residual of each of the discrete equation are less than 10^{-4}.

3.3 Experimental Setup and Simulation Model

Figure 10a shows the autoclave used in experiment has an inner cavity with the size of 3 m in length and 1.2 m in diameter. The mean flow velocity of air in this used autoclave is approximately 4 m/s and the range of pressure is 0–1.5 MPa. During the autoclave process, the manufactured mold (as shown in Fig. 7) is placed midway within autoclave without a gap with the trolley working plane. The measurements of temperature curves are conducted by means of a calorimeter with four thermocouples (type K, accuracy ± 1 °C). As shown in Fig. 10b, three thermocouples P1, P2, and P3 are diagonally placed on the mold plate. Another thermocouple P4 is located in the front of the autoclave to monitor the air temperature. Each measurement point provides a temperature value every ten seconds.

Figure 11 shows the two-dwelling temperature profile used in the experiment and simulation. The first and second heating rates are both 1.8 K/min, the first dwelling is 333 K for 50 min, and the second dwelling is 398 K for 120 min. The cooling stage is not considered in the simulation. The pressure is holding at 0.6 MPa during the entire cycle.

The mesh of the simulation model is shown in Fig. 12. Concerning the irregular shape of the mold, unstructured mesh is selected for its excellent adaptability. As shown in Fig. 12,
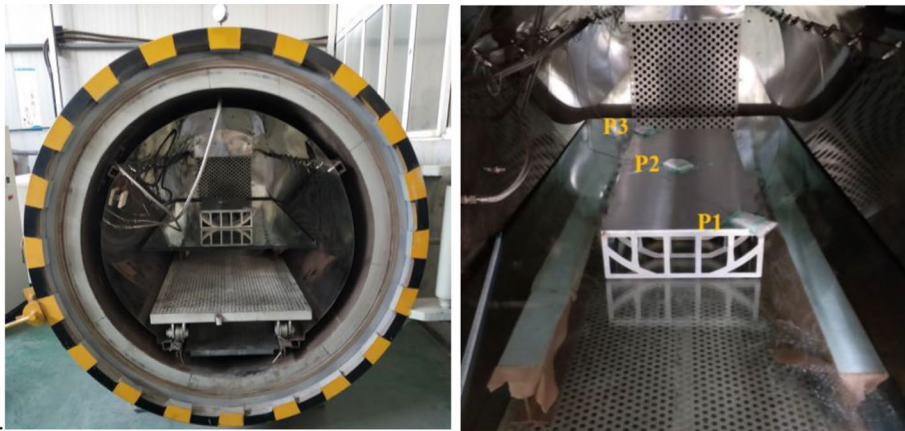
**(a)** Autoclave   **(b)** Locations of thermocouples

Fig. 10 The experiment setup

a mixed mesh of tetrahedral and hexahedral grid is adopted in the fluid domain with three prism layers surrounding the mold. The mesh near the fluid–solid interface is refined asymptotically for higher calculation accuracy.

The temperature profile in Fig. 11 is applied at the inlet of the autoclave by writing the temperature function in user defined function (UDF). The average flow velocity is set to 4 m/s. A uniform pressure recommend in Fig. 11 is applied in the entire fluid domain. At the outlet of the autoclave, a static pressure with the value of 0 is applied. The wall of the autoclave is usually made of a thermally insulating material and is relatively thick. Therefore, the boundary of the external wall is assumed to be adiabatic.

The thermophysical properties of air and aluminum alloy 6061 are considered as constant and displayed in Table 2. The Reynolds number of air flow Re > 12000 (calculated by Eq. (11)). Therefore, the flow is turbulent, and the k-Epsilon turbulent model is adopted in the fluid domain.

Fig. 11 Temperature and pressure profiles of experiment
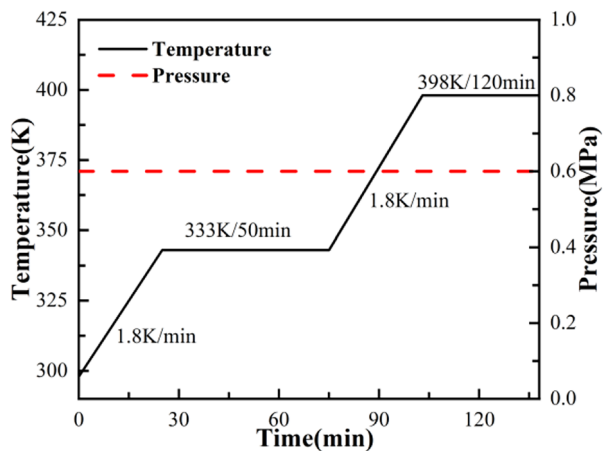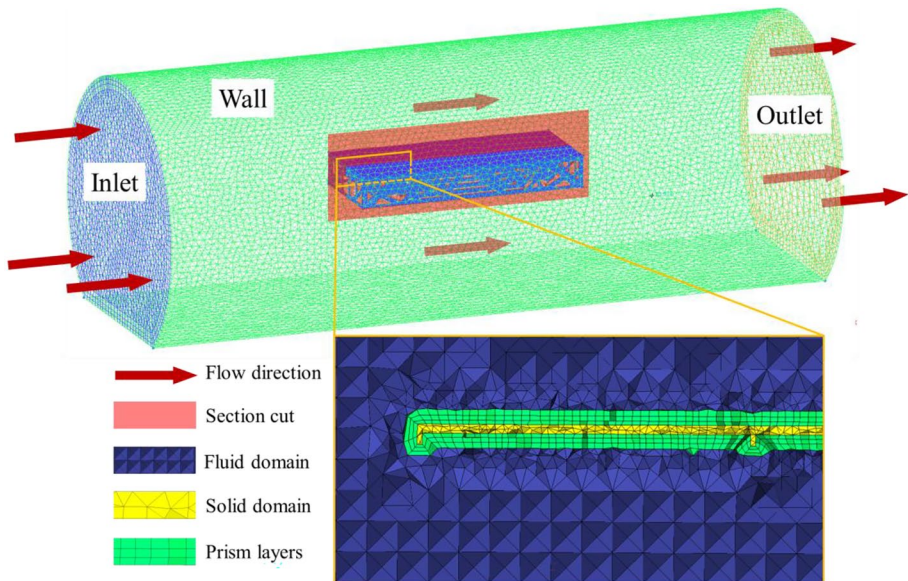
Fig. 12 Mesh of the autoclave system

3.4 Comparison of the Simulated and Experimental Results

The temperature curves obtained by simulation and experiment at the positions P1, P2, and P3 are illustrated in Fig. 13a. It is observed that the temperature evolution trends have great agreements at these points. The temperature rising curves of the measurement points all lag behind that of air. In both of the two heating stages, the temperature rises slowly at the beginning and then accelerates until a steady heating rate. This is because the convection effect inside the autoclave is not obvious at the initial stage of heating, and the heat transfer tends to be stable after a period of time. An obvious temperature difference is found while just reaching the preserving stage and it is declined gradually after a while.

Figure 13b displays the temperature errors between the numerical and experimental results at the three points. It is seen that the errors rise with the increase of distance between the measurement point and autoclave door. For each point, the maximum deviation occurs at the end of the second heating stage. The maximum error is 4.5%, which highlights the predictive capacity of the proposed simulation model for predicting the temperature distribution of the mold in autoclave.

Table 2 Thermophysical properties of air and aluminum alloy 6061

| Parameters	Air	Aluminum
Density/(kg·m-3)	1.185	2750
Viscosity/(kg·m-1·s-1)	$1.83 \times 10{-}5$	–
Heat capacity/(J·kg-1·K-1)	1004.4	896
Conductivity/(W·m-1·K-1)	0.0261	154
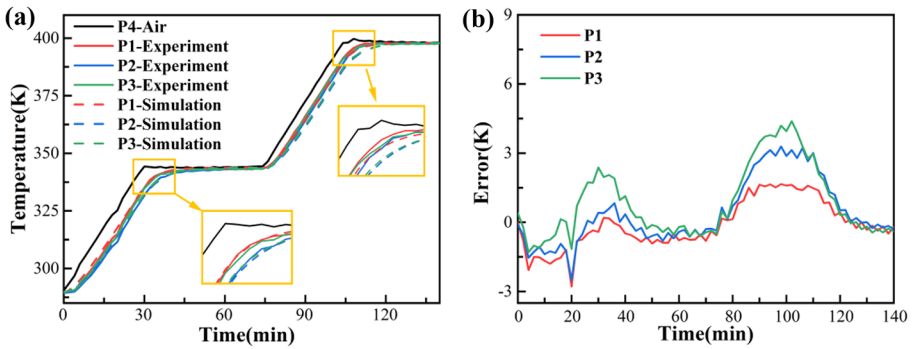
Fig. 13 Comparison of the simulated and experimental temperature results at the three measurement points P1, P2, P3. **a** the temperature history curves; **b** the temperature error history curves

3.5 Comparison of the Temperature Uniformity of the Original and Optimized Mold

The verified simulation model is then applied to compute the temperature distribution of the original and optimized mold in autoclave. In order to save the computation cost, only the heating process with a heating rate of 0.05 K/s is considered in the simulation. The autoclave applied in this study has the size of 10 m in length and 3 m in diameter. The other conditions are the same as the model in Sect. 3.3.

The computed velocities of fluid flow along the center plane of the autoclave are presented in Fig. 14. In both two molds, the velocity near the top of the mold is higher than that at the bottom and an obvious velocity gradient occurs at the fluid–solid interface. When air passes through the inside of the molds, the flow velocity slows down gradually from the front to the back of support structure and eddies are generated. However, it is clear seen that the flow velocity inside the optimized mold is much higher than the
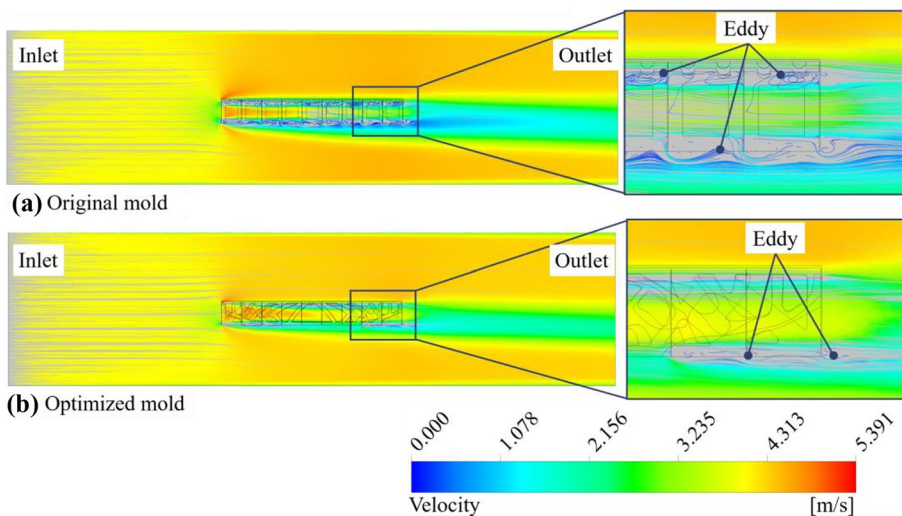
Fig. 14 Computed velocities of fluid flow along the center plane of the autoclave for the two molds

original mold. The faster air convection means the more efficient heat transfer between the fluid and mold. Hence, these results indirectly indicate that the topology optimized mold has a better heat transfer performance during autoclave process.

Figure 15 displays the comparison of the mold plates temperature for the original and optimized molds. In Fig. 15a, the maximum temperature difference reaches 26.9 K with the original mold, while it is only 19.1 K with the optimized mold. The mold plate temperature distributions at the end of heating are presented in Fig. 15b and c. It is seen that the highest temperature of the two mold plates both occurs at the border of the windward side. However, the locations of the lowest temperature have a clear distinction due to the different support structures. A reduction of thermal gradient by 7.8 K is accomplished and the mold temperature uniformity is enhanced by 29%. As expected, a mold structure with better thermal performance is obtained by employing the topology optimization approach.
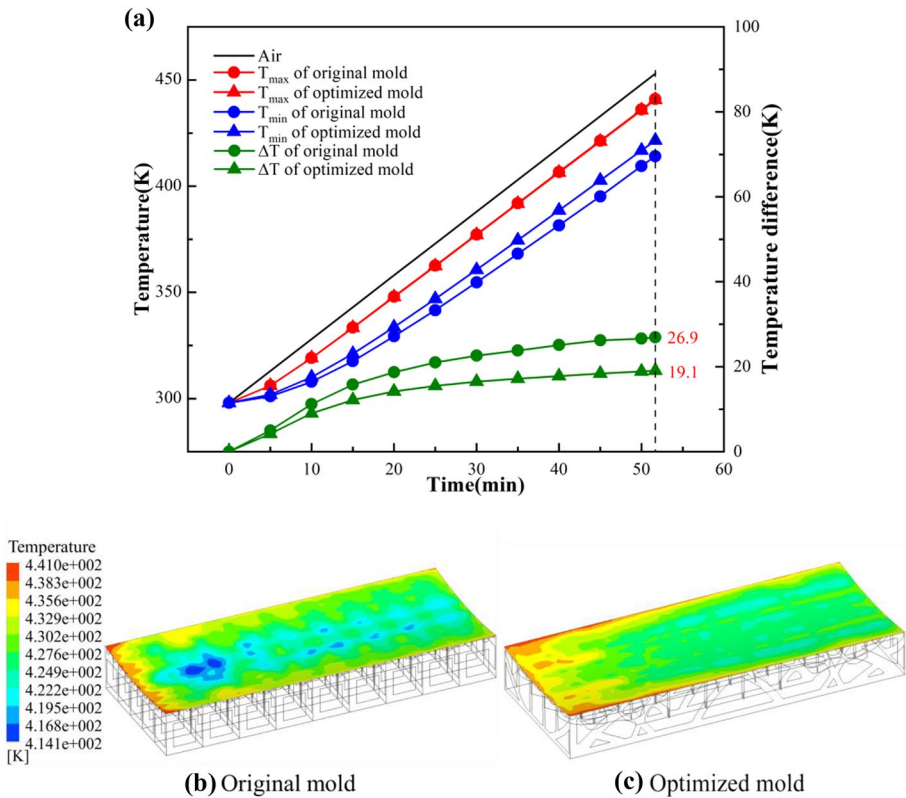
Fig. 15 Comparison of temperature results of the two mold plates. **a** the maximum temperature T_{max}, minimum temperature T_{min}, and temperature difference ΔT history curves; **b** and **c** the temperature distributions at the end of the heating stage
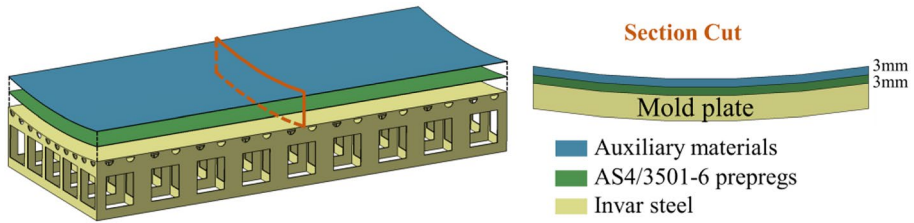
Fig. 16 Schematic of the simulated model of the curing process

4 Effect of Optimized Mold on the Synchronization of Curing

4.1 Numerical Model

Besides the effect of mold, the auxiliary materials covered on the mold decrease the heat transfer rate between the air and composite part. And the internal reaction heat occurs in the composite part during curing process [35]. Thus, to further explore the effect of the optimized mold on the curing performance of composite panel, the numerical model combining the mold, composite prepregs and auxiliary materials is developed to simulate the curing process.

In this study, the phenomenological model of the cure kinetics is adopted to represent the curing process by a rate equation. The AS4/3501–6 composite is concerned and its cure kinetics equation [36] is expressed as:

$$\frac{d\alpha}{dt} = \begin{cases} (K_1 + K_2\alpha)(1-\alpha)(0.47-\alpha) & (\alpha \le 0.3) \\ K_3(1-\alpha) & (\alpha > 0.3) \end{cases} \tag{13}$$

where α represents DoC, $\frac{d\alpha}{dt}$ is the instantaneous cure rate, K_i ($i = 1, 2, 3$) is the curing rate constant which can be defined by the Arrhenius equations:

$$K_i = A_i \exp(\frac{-\Delta E_i}{RT}) \ (i = 1, 2, 3) \tag{14}$$

where R is the universal gas constant, A_i is the frequency factor obtained from experiments and ΔE_i is the activation energy.

The internal heat $\dot{q}$ released in the cure reaction, which can be quantitatively expressed as:

$$\dot{q} = \rho_r V_r H_r \frac{d\alpha}{dt} \tag{15}$$

Table 3 Thermophysical properties of AS4/3501–6 prepregs and auxiliary materials

Parameters	Density/(kg·m^{-3})	Specific heat/(J·kg^{-1}·K^{-1})	Conductivity/(W·m^{-1}·K^{-1})
Auxiliary materials	423	1025	0.07
AS4/3501–6 prepregs	1520	942	0.4459

Table 4 Cure kinetics parameters of 3501–6 epoxy resin [37]

| Parameters	Value	Parameters	Value
A_1/s^{-1}	3.502×10^7	$\Delta E_1/(J \cdot mol^{-1})$	8.07×10^4
A_2/s^{-1}	-3.357×10^7	$\Delta E_2/(J \cdot mol^{-1})$	7.78×10^4
A_3/s^{-1}	3.267×10^7	$\Delta E_3/(J \cdot mol^{-1})$	5.66×10^4
$R/(J \cdot mol^{-1} \cdot K^{-1})$	8.3143	$H_r/(J \cdot kg^{-1})$	473600

where ρ_r is the density of the resin, V_r is the volume fraction of the resin, H_r is the heat generated by the complete reaction of unit mass of resin. The Eqs. (15)–(17) are further introduced into Eq. (12) to evaluate the internal heat S_T generated by the exothermic reaction of resin curing.

The simulated model is schematically shown in Fig. 16. The mold is covered by the composite panel and auxiliary materials. The thickness of composite panel is 3 mm. Auxiliary materials consisting of the vacuum bag and porous Teflon and bleeder, are combined into an effective layer with the thickness of 3 mm and covered on the composite panel. For simplifying the simulation model, some assumptions are proposed as below:

(a) All material properties are independent of temperature;
(b) Heat caused by viscous dissipation is neglected;
(c) The heat transfer of the contact surfaces between the separate parts of the model is considered optimal.

The equivalent thermal physical properties of the auxiliary materials [14] and AS4/3501–6 composite are listed in Table 3. The cure kinetics parameters of 3501–6 epoxy resin are listed in Table 4.
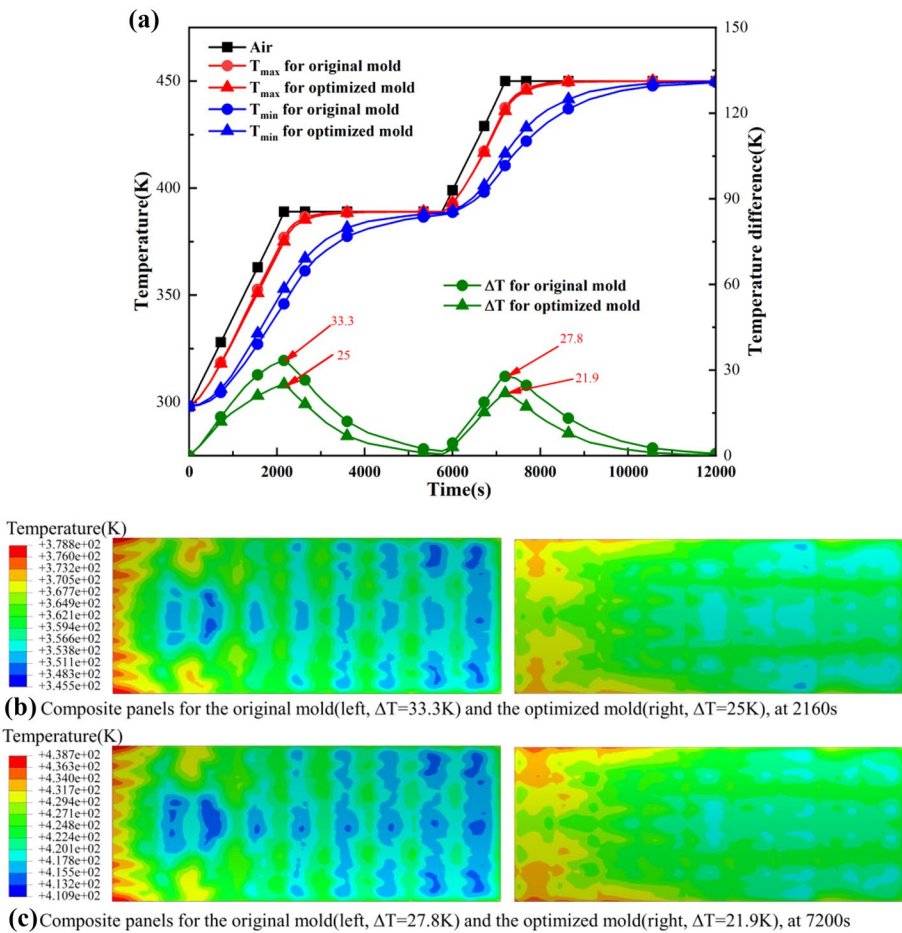
The curing cycle [38] of AS4/3501–6 prepregs is displayed in Fig. 17. The temperature profile is applied at the inlet of the autoclave by writing the temperature function in UDF. A unique heat source is applied in the composite by defining the curing reaction function in UDF. The average flow velocity is set to 4 m/s. A uniform pressure recommend in Fig. 17 is applied in the entire fluid domain.

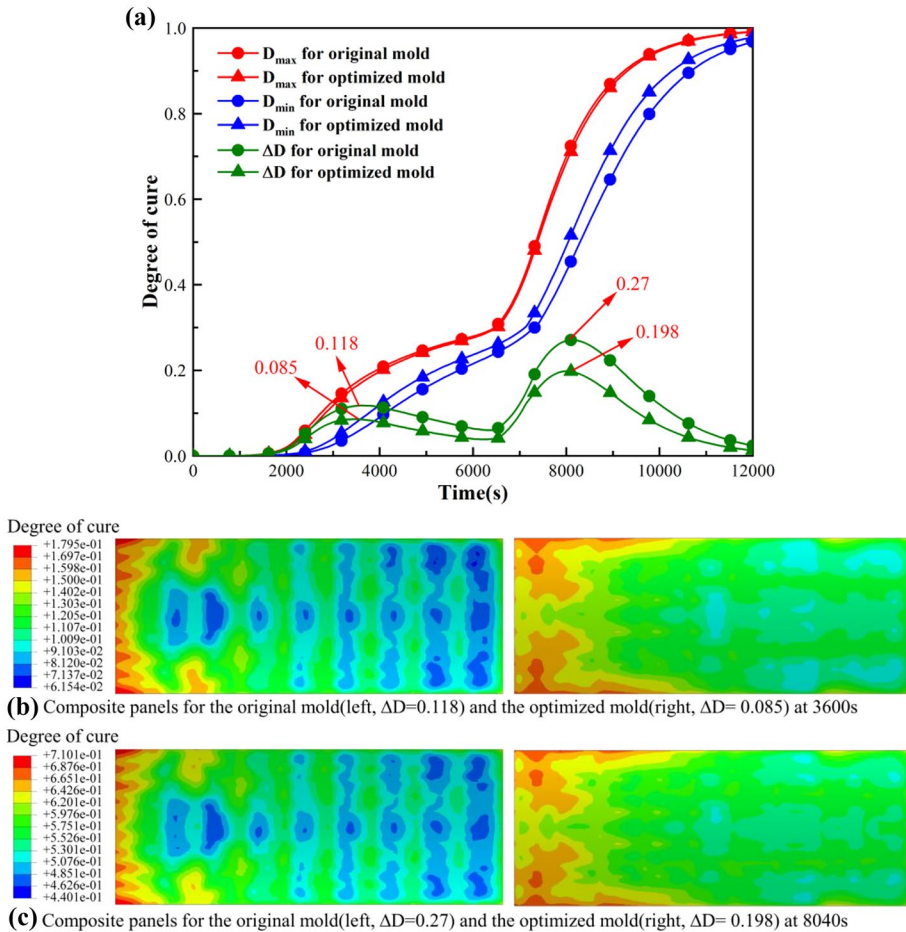**Fig. 17** Curing cycle of AS4/3501–6 prepregs
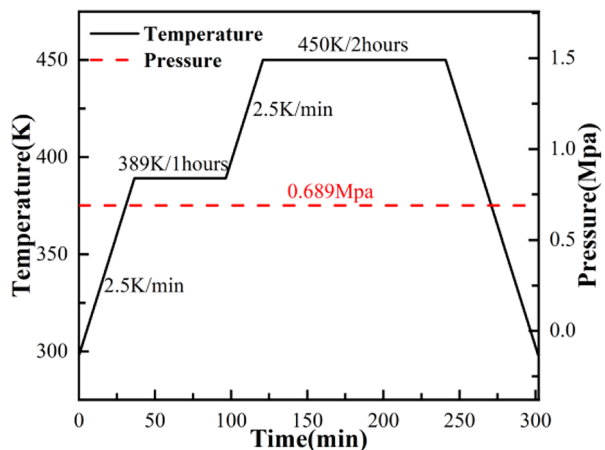
4.2 Results and Discussion

Figure 18 shows the simulation results of the temperature of the composite panels for original and optimized molds during the first 12000 s of the curing cycle displayed in Fig. 17. As shown in Fig. 18a, the obvious temperature differences are both observed at the end of the two heating stages. The temperature distributions of the composite panels at the end of first and second heating stages are presented in Fig. 18b and c respectively. Compared to the original mold, the maximum deviation of temperature ΔT within the composite panel for optimized mold is reduced by 24.9% and 21.2%, respectively at the end of the first and second heating stages.

Figure 19 shows the simulation results of the DoC of the composite panels for original and optimized molds during the first 12000 s of the curing cycle. In Fig. 19a, two peaks of the maximum deviation of DoC ΔD, are appeared at the initial stages of the first and second dwelling. Although the maximum ΔT is occurred at the end of the first heating stage,

(b) Composite panels for the original mold(left, ΔT=33.3K) and the optimized mold(right, ΔT=25K), at 2160s

(c) Composite panels for the original mold(left, ΔT=27.8K) and the optimized mold(right, ΔT=21.9K), at 7200s

Fig. 18 Comparison of the temperature results of the composite panels for the two molds. **a** the maximum temperature T_{max}, minimum temperature T_{min}, and temperature difference ΔT history curves; **b** and **c** the temperature distributions at the end of the first and second heating stages

(a)

(b) Composite panels for the original mold(left, ΔD=0.118) and the optimized mold(right, ΔD= 0.085) at 3600s

(c) Composite panels for the original mold(left, ΔD=0.27) and the optimized mold(right, ΔD= 0.198) at 8040s

Fig. 19 Comparison of the DoC results of the composite panels for the two molds. **a** the maximum DoC D_{max}, minimum DoC D_{min}, and DoC difference ΔD history curves; **b** and **c** the DoC distributions at two peaks

the first peak of ΔD is much lower than the second one due to the slow curing rate at the preliminary stage of curing. The DoC distributions of composite panels with the peaks of ΔD are displayed in Fig. 19b and c. Compared to the original mold, the maximum deviation of DoC ΔD in composite panel for the optimized mold is reduced by 26.7%. Thus, the synchronism of curing has been significantly improved by redesigning the mold structure. It further proves the topology optimization method proposed in this paper is efficient to promote the thermal performance of frame mold.

5 Conclusions

In this study, important factors influencing the performance of mold in an autoclave are identified, and it is believed that the structure of mold is of great importance. A topology optimization approach is presented here for designing the autoclave mold structure with low

weight, high stiffness and temperature uniformity. Firstly, a topology optimization model of mold is formulated, and a novel substructure is obtained and manufactured. Compared with the original mold, the optimized mold increases the stiffness and reduces the total weight. Then, to evaluate the temperature uniformity of the optimized mold, a CFD simulation of autoclave process is conducted. And the experiment in an autoclave is performed to validate the numerical results. The simulation results show that the temperature uniformity of the optimized mold is obviously improved. Furthermore, the effect of auxiliary materials and reaction heat of composites are added to the simulation model to compute the DoC of the composite panel. The results indicate that better synchronism of curing is realized by the topology design of mold. It is shown that the topology optimization technique in the mold design is feasible for the manufacturing of large composite components and shows enough potential in practical applications.

Authors' Contributions Bo Yue: Methodology, Software, Experiment, Validation, Investigation, Writing–original draft, Supervision. Yingjie Xu: Conceptualization, Resources, Writing–Review & Editing, Project administration, Funding acquisition. Weihong Zhang: Resources, Writing–Review & Editing, Supervision, Funding acquisition.

Availability of Data and Material The authors confirm that the data supporting the findings of this study are available within the article.

Code Availability Not applicable.

Declarations

Ethics Approval Work was conducted ethically with no human test subjects.

Consent to Participate Not applicable.

Consent for Publication All the authors give their consent for the publication of this article.

Competing Interests The authors declare that they have no known competing financial interests or personal relationships that could have appeared to influence the work reported in this paper.

References

1. Upadhya, A., Dayananda, G., Kamalakannan, G., Ramaswamy, S., Christopher, D.J.: Autoclaves for aerospace applications: issues and challenges. Int. J. Aerosp. Eng. **2011**, 985871 (2011). https://doi.org/10.1155/2011/985871
2. Mirzaei, S., Krishnan, K., Al Kobtaw, C., Roberts, J., Palmer, E.: Heat transfer simulation and improvement of autoclave loading in composites manufacturing. Int. J. Adv. Manuf. Technol. **112**, 2989–3000 (2021). https://doi.org/10.1007/s00170-020-06573-3
3. Hudek, M.: Examination of heat transfer during autoclave processing of polymer composites. University of Manitoba, Canada (2001) (Master's Thesis)
4. Athanasopoulos, N., Koutsoukis, G., Vlachos, D., Kostopoulos, V.: Temperature uniformity analysis and development of open lightweight composite molds using carbon fibers as heating elements. Compos. Part. B. Eng. **50**, 279–289 (2013). https://doi.org/10.1016/j.compositesb.2013.02.038
5. Pusatcioglu, S., Hassler, J., Fricke, A., Mcgee, H.: Effect of temperature gradients on cure and stress gradients in thick thermoset castings. J. Appl. Polym. Sci. **25**, 381–393 (1980). https://doi.org/10.1002/app.1980.070250305

6. Johnston, A.: An integrated model of the development of process-induced deformation in autoclave processing of composite structures. University of British Columbia, Canada (1997) (Ph.D. thesis)
7. Ding, A., Li, S., Wang, J., Zu, L.: A three-dimensional thermo-viscoelastic analysis of process-induced residual stress in composite laminates. Compos. Struct. **129**, 60–69 (2015). https://doi.org/10.1016/j.compstruct.2015.03.034
8. Gopal, A., Adali, S., Verijenko, V.: Optimal temperature profiles for minimum residual stress in the cure process of polymer composites. Compos. Struct. **48**, 99–106 (2000). https://doi.org/10.1016/S0263-8223(99)00080-X
9. Wang, Q., Yang, X., Zhao, H., Zhang, X., Cao, G., Ren, M.: Microscopic residual stresses analysis and multi-objective optimization for 3D woven composites. Compos. Part. A. Appl. Sci. Manuf. **144**, 106310 (2021). https://doi.org/10.1016/j.compositesa.2021.106310
10. Wang, Q., Li, T., Yang, X., Wang, K., Wang, B., Ren, M.: Prediction and compensation of process-induced distortions for L-shaped 3D woven composites. Compos. Part. A. Appl. Sci. Manuf. **141**, 106211 (2021). https://doi.org/10.1016/j.compositesa.2020.106211
11. Han, N., An, L., Fan, L., Hua, L., Gao, G.: Research on temperature field distribution in a frame mold during autoclave process. Materials. **13**, 4020 (2020). https://doi.org/10.3390/ma13184020
12. Chen, F., Zhan, L., Li, S.: Refined simulation of temperature distribution in molds during autoclave process. Iran. Polym. J. **25**, 775–785 (2016). https://doi.org/10.1007/s13726-016-0466-0
13. Dolkun, D., Wang, H., Wang, H., Ke, Y.: An efficient thermal cure profile design method for autoclave curing of large size mold. Int. J. Adv. Manuf. Technol. **114**, 2499–2514 (2021). https://doi.org/10.1007/s00170-021-07015-4
14. Xie, G., Liu, J., Zhang, W., Sunden, B.: Simulation and thermal analysis on temperature fields during composite curing process in autoclave technology. ASME International Mechanical Engineering Congress and Exposition, Houston (2012). https://doi.org/10.1115/IMECE2012-85918
15. Xie, G., Liu, J., Zhang, W., Lorenzini, G., Biserni, C.: Simulation and improvement of temperature distributions of a framed mould during the autoclave composite curing process. J. Eng. Thermophys. **22**, 43–61 (2013). https://doi.org/10.1134/S1810232813010062
16. Zhang, G., Zhang, B., Luo, L., Lin, T., Xue, X.: Influence of mold and heat transfer fluid materials on the temperature distribution of large framed molds in autoclave process. Materials. **14**, 4311 (2021). https://doi.org/10.3390/ma14154311
17. Weber, T., Arent, J., Munch, L., Duhovic, M., Balvers, J.: A fast method for the generation of boundary conditions for thermal autoclave simulation. Compos. Part. A. Appl. Sci. Manuf. **88**, 216–225 (2016). https://doi.org/10.1016/j.compositesa.2016.05.036
18. Telikicherla, M., Altan, M., Lai, F.: Autoclave curing of thermosetting composites: process modeling for the cure assembly. Int. Commun. Heat. Mass. Transf. **21**, 785–797 (1994). https://doi.org/10.1016/0735-1933(94)90032-9
19. Zhang, C., Wang, Y., Liang, X., Zhang, B., Yue, G., Jiang, P.: Research with CFX software on frame mould temperature field simulation in autoclave process. Polym. Polym. Compos. **17**(5), 325–336 (2009). https://doi.org/10.1177/096739110901700506
20. Wang, Q., Wang, L., Zhu, W., Xu, Q., Ke, Y.: Design optimization of molds for autoclave process of composite manufacturing. J. Reinf. Plast. Comp. **36**, 1564–1576 (2017). https://doi.org/10.1177/0731684417718265
21. Wang, L., Zhu, W., Wang, Q., Xu, Q., Ke, Y.: A heat-balance method for autoclave process of composite manufacturing. J. Compos. Mater. **53**, 641–652 (2019). https://doi.org/10.1177/0021998318788918
22. Bendsoe, M., Kikuchi, N.: Generating optimal topologies in structural design using a homogenization method. Comput. Methods. Appl. Mech. Eng. **71**, 197–224 (1988). https://doi.org/10.1016/0045-7825(88)90086-2
23. Sigmund, O., Maute, K.: Topology optimization approaches. Struct. Multidisc. Optim. **48**, 1031–1055 (2013). https://doi.org/10.1007/s00158-013-0978-6
24. Qiu, Z., Li, Q., Luo, Y., Liu, S.: Concurrent topology and fiber orientation optimization method for fiber-reinforced composites based on composite additive manufacturing. Comput. Methods. Appl. Mech. Eng. **395**, 114962 (2022)
25. Zhu, J., Zhang, W., Xia, L.: Topology Optimization in aircraft and aerospace structures design. Arch. Computat. Methods. Eng. **2**, 595–622 (2016). https://doi.org/10.1007/s11831-015-9151-2
26. Bendsøe, M.: Optimal shape design as a material distribution problem. Struct. Optim. **1**, 193–202 (1989). https://doi.org/10.1007/BF01650949
27. Bendsøe, M., Sigmund, O.: Topology optimization: theory, method and applications. Springer, Berlin (2004)
28. Sigmund, O., Peterssonm, J.: Numerical instabilities in topology optimization: a survey on procedures dealing with checkerboards, mesh-dependencies and local minima. Struct. Optim. **16**, 68–75 (1998). https://doi.org/10.1007/BF01214002

29. Bruns, T., Tortorelli, D.: Topology optimization of nonlinear elastic structures and compliant mechanisms. Comput. Methods. Appl. Mech. Eng. **190**, 3443–3459 (2001). https://doi.org/10.1016/S0045-7825(00)00278-4

30. Nan, J., Li, G., Xu, K.: Yielding behavior of low expansion invar alloy at elevated temperature. J. Mater. Process. Tech. **114**, 36–40 (2001). https://doi.org/10.1016/S0924-0136(01)00732-4

31. Gibbons, G., Wimpenny, D.: Mechanical and thermomechanical properties of metal spray invar for composite forming tooling. J. Mater. Eng. Perform. **9**, 630–637 (2000). https://doi.org/10.1361/105994900770345485

32. Monaghana, P., Broganb, M., Oosthuizenc, P.: Heat transfer in an autoclave for processing thermoplastic composites. Compos. Manuf. **2**, 233–242 (1991). https://doi.org/10.1361/105994900770345485

33. Slesinger, N., Shimizu, T., Arafath, A., Poursartip, A.: Heat transfer coefficient distribution inside an autoclave. In: 17th International conference on composite material ICCM, Edinburgh, UK. https://www.researchgate.net/publication/282661644_HE (2009). Accessed 27-31 July 2009

34. Kluge, J., Lundstrom, T., Westerberg, L., Nyman, T.: Modelling heat transfer inside an autoclave: effect of radiation. J. Reinf. Plast. Comp. **35**, 1126–1142 (2016). https://doi.org/10.1177/0731684416641333

35. Amiri, D., Emamian, A., Sajjadi, H., Atashafrooz, M., Li, Y., Wang, L., Jing, D., Xie, G.: A Comprehensive review on multi-dimensional heat conduction of multi-layer and composite structures: analytical solutions. J. Therm. Sci. **30**, 1875–1907 (2021). https://doi.org/10.1007/s11630-021-1517-1

36. White, S., Hahn, H.: Process modeling of composite materials: residual stress development during cure. I - model formulation. J. Compos. Mater. **26**, 2402–2422 (1992). https://doi.org/10.1177/002199839202601604

37. Lee, W., Loos, A., Springer, G.: Heat of reaction, degree of cure, and viscosity of Hercules 3501–6 resin. J. Compos. Mater. **16**, 510–520 (1982). https://doi.org/10.1177/002199838201600605

38. Yuan, Z., Wang, Y., Yang, G., Tang, A., Yang, Z., Li, S., Li, Y., Song, D.: Evolution of curing residual stresses in composite using multi-scale method. Compos. Part. B. Eng. **155**, 49–61 (2018). https://doi.org/10.1016/j.compositesb.2018.08.012